

# Inclusive Photoproduction of $D^*$ Mesons with Massive Charm Quarks

G. Kramer<sup>1</sup> and H. Spiesberger<sup>2</sup>

<sup>1</sup> II. Institut für Theoretische Physik, Universität Hamburg,  
Luruper Chaussee 149, D-22761 Hamburg, Germany

<sup>2</sup> Institut für Physik, Johannes-Gutenberg-Universität,  
Staudinger Weg 7, D-55099 Mainz, Germany

## Abstract

We have calculated the next-to-leading order cross sections for the inclusive production of  $D^*$  mesons in  $\gamma p$  collisions at HERA in two approaches using massive or massless charm quarks. The usual massive theory for the direct cross section with charm quarks only in the final state was transformed into a massive theory with  $\overline{\text{MS}}$  subtraction by subtracting the mass divergent and additional finite terms calculated earlier in connection with the process  $\gamma\gamma \rightarrow D^* X$ . This theory approaches the massless theory with increasing transverse momentum. The difference between the massive and the massless approach with  $\overline{\text{MS}}$  subtraction is studied in detail in those kinematic regions relevant for comparison with experimental data. With these results and including the resolved cross section which is dominated by the part originating from the charm in the photon, we compute the fully inclusive  $D^{*\pm}$  cross section and compare it with recent preliminary data from the ZEUS collaboration at HERA. We find on average good agreement.

# 1 Introduction

$D^*$  production in high-energy  $ep$  collisions at HERA is dominated by photoproduction where the electron (positron) is scattered by a small angle producing photons of almost zero virtuality ( $Q^2 \simeq 0$ ). At leading order (LO) of perturbative QCD, the main process for  $\gamma + p \rightarrow D^* + X$  is photon-gluon fusion. Here the photon interacts directly with the gluon ( $g$ ) from the proton producing a charm-anticharm quark pair in the final state ( $\gamma + g \rightarrow c + \bar{c}$ ), from which the  $c$  or  $\bar{c}$  fragment into  $D^{*+}$  or  $D^{*-}$  mesons, respectively. Besides the direct photoproduction channel,  $D^*$  production at HERA can proceed also via the resolved photoproduction process. In this case, the photon acts as a source of partons which interact with the partons in the proton, as for example in the process  $\gamma + p \rightarrow g + g \rightarrow c + \bar{c}$ .

It is well-known that LO QCD predictions are not reliable and next-to-leading order (NLO) calculations are needed. Two distinct approaches for NLO calculations have been used to obtain predictions for charm-quark production. In the so-called massive charm approach, also called fixed flavor-number scheme (FFN) [1], one assumes that the gluon and light quarks ( $u, d, s$ ) are the only active partons within the proton and the photon (in the case of the resolved contribution). The charm quark appears only in the final state of the direct and resolved processes via the hard scattering of light partons including the photon into  $c\bar{c}$  pairs. In this case, the  $c$  quark is always treated as a heavy particle and never as a parton. The charm mass  $m$  is explicitly taken into account along with the transverse momentum  $p_T$  of the produced  $D^*$  as if they were of the same order, irrespective of their true relative magnitudes. In this scheme, the charm mass acts as a cutoff for the initial- and final-state collinear singularities and sets the scale for the perturbative calculations. However, at NLO, terms  $\propto \alpha_s \ln(p_T^2/m^2)$  arise from collinear emissions of a gluon by the charmed quark at large transverse momenta or from almost collinear branchings of photons or gluons into  $c\bar{c}$  pairs. These terms are of order  $O(1)$  for large  $p_T$  and with the choice  $\mu_R \sim p_T$  for the renormalization scale they spoil the convergence of the perturbation series. The FFN approach with  $n_f = 3$  should thus be limited to a rather small range of  $p_T \sim m$ . Nevertheless, predictions in this approach have been compared to experimental data up to  $p_T = 20$  GeV [2, 3].

The other calculational scheme which has been applied to the process  $\gamma + p \rightarrow D^* + X$  is the so-called massless scheme (ZM scheme) [4, 5, 6], which is the conventional parton model approach. In this scheme, the zero-mass parton approximation is applied also to the charm quark, although its mass  $m$  is certainly much larger than  $\Lambda_{QCD}$ . Here the charm quark is also an ingoing parton originating from the proton or the photon, leading to additional direct and resolved contributions (besides those from incoming  $u, d, s$  quarks and the gluon  $g$ ). The charm quark fragments into the  $D^*$  meson similarly as the light quarks and the gluon with a fragmentation function (FF) known from other processes. The well-known factorization theorem then provides a straightforward procedure for incorporating this FF into the order-by-order perturbative calculation. Although this approach can be used as soon as the factorization scales of initial and final state are above the starting

scale of the parton distribution functions (PDF) of the photon and the proton and of the FF of the  $D^*$ , the predictions are expected to be reliable only in the region of large transverse momenta  $p_T \gg m$ , since terms of the order of  $m^2/p_T^2$  are neglected.

At many places in the literature, mostly in the context of charm production in deep inelastic  $ep$  scattering (for a recent review see [7]), it has been explained that the correct approach for  $p_T \gg m$  is to absorb the potentially large logarithms that occur in the FFN approach, into the charm PDFs of the proton and the photon and into the FF of the  $c$  into  $D^*$ . Then, large logarithms  $\propto \ln(M^2/m^2)$ , defined with the factorization scale  $M$ , determine the evolution to higher scales and can be resummed with the help of the DGLAP evolution equations for the PDFs and FFs. The unsubtracted terms  $\propto \ln(p_T^2/M^2)$  are of order  $O(1)$  for the appropriate choice  $M$  of order  $p_T$ . The remaining dependence on  $m$ , i.e. the terms proportional to  $m^2/p_T^2$ , can be kept in the hard cross section to achieve a better accuracy in the intermediate region  $p_T \gtrsim m$ . The factorization of the logarithmic terms in  $m^2$  can be extended consistently to higher orders in  $\alpha_s$ , as has been shown by Collins in the context of heavy quark production in high- $Q^2$   $ep$  collisions [8]. Keeping all terms proportional to  $m^2/p_T^2$  in the hard scattering cross section allows one to use massless coefficient functions to obtain the transition from the factorization scale  $m^2$  in the original FFN cross section to the factorization scale  $M^2$ .

The subtraction of the collinearly, i.e. mass, singular terms does not define a unique factorization scheme. Also the finite terms must be specified. In the ZM calculations the mass  $m$  is set to zero from the beginning and the collinearly divergent terms are defined with dimensional regularization and  $\overline{\text{MS}}$  subtraction by convention. The chosen regularization and subtraction procedure also fixes the finite terms. If, on the other hand, one starts with  $m \neq 0$  and performs the limit  $m \rightarrow 0$  afterwards, the finite terms can be different. These finite terms must be removed by subtraction together with the  $\ln m^2$  terms so that in the limit  $p_T \rightarrow \infty$  the known massless  $\overline{\text{MS}}$  expressions are recovered. This requirement is mandatory since the existing PDFs and FFs, including those for heavy quarks, are defined in this particular scheme. The subtraction scheme defined in this way is the appropriate extension of the conventional ZM scheme to include charm mass effects in a consistent way. Actually, just recently PDFs of the proton with heavy quark mass effects included have been constructed by the CTEQ group [9, 10]. If these would be used in a calculation of charm production in  $\gamma p$  collisions, the factorization procedure of the corresponding hard scattering cross section must be adjusted to these heavy quark PDFs. In the moment this would be premature as long as similar constructions for the charm PDF of the photon at NLO and similarly for the FF for  $c \rightarrow D^*$  do not exist.

In a recent work we applied this finite charm mass scheme with  $\overline{\text{MS}}$  subtraction, as outlined above, to the calculation of the cross section for  $\gamma + \gamma \rightarrow D^* + X$  [11]. The single-resolved cross section for this process, where one of the photons is resolved and the other is direct, is, except for the replacement of the photon PDF by the proton PDF, the same as for the direct contribution of the reaction  $\gamma + p \rightarrow D^* + X$ . Therefore the subtraction terms needed for the evaluation in the  $\overline{\text{MS}}$  ZM scheme, established in our previous work, can be directly taken over to the calculation of the direct photoproduction cross section. This

direct cross section plays an important role due to the partonic subprocesses  $\gamma + g \rightarrow c + \bar{c}$  at LO and  $\gamma + q \rightarrow c + \bar{c} + q$  at NLO, where  $q$  is one of the light (massless) quarks. These contributions, and the NLO corrections to the photon-gluon fusion process, are calculated with massive  $c$  quarks.

In addition we have the contributions due to  $\gamma + c \rightarrow c + g$  and its NLO corrections as part of the direct cross section with  $n_f = 4$  flavors. These contributions are evaluated with  $m = 0$  in the hard scattering cross section to be consistent with the chosen PDF of the proton as mentioned above. The particular prescription for the treatment of the incoming charm quark in the direct and also in the resolved contribution as a massless parton is in fact unavoidable. Since the charm PDFs we are going to use are determined with  $m = 0$  in the hard scattering cross sections, this is the only consistent choice. The finite charm mass appears only in the starting scale  $\mu_0 = 2m$  with the effect that the charm PDF vanishes below the scale  $\mu_0$ . Actually this prescription is also applied in the treatment of heavy quark effects in deeply inelastic scattering as in the recent work [10] and was suggested earlier [8, 12, 7].

The resolved cross section for  $\gamma + p \rightarrow D^* + X$  is dominated by the part in which the photon resolves into a  $c$  quark (or  $\bar{c}$  antiquark). This part is calculated with  $m = 0$ , in the same way as in the contribution where the proton resolves into  $c$  ( $\bar{c}$ ). The resolved parts with  $c$  ( $\bar{c}$ ) only in the final state coming from  $q + \bar{q} \rightarrow c + \bar{c}$  and  $g + g \rightarrow c + \bar{c}$  and the corresponding NLO corrections together with  $g + q \rightarrow c + \bar{c} + q$  are very small, in particular for larger  $p_T$ 's. As we shall see, for  $p_T \geq 3$  GeV it amounts to only a few percent of the complete cross section. Due to the smallness of this contribution, it will be considered in the ZM four-flavor approach.

It is the purpose of this work to incorporate the non-zero charm mass effects into the predictions for  $\gamma + p \rightarrow D^* + X$ , following very closely our previous work [11] on inclusive  $D^*$  production in  $\gamma\gamma$  collisions, in order to discover those kinematic regions in which the charm mass is important. A different approach to correct the usual ZM approximation by non-zero charm mass effects is the so-called FONLL (fixed order plus NLO logarithms) approach [13].

The outline of the paper is as follows. In Sect. 2 we study the difference between the four-flavor massive and the massless approach more closely by looking at cross sections in different kinematic regions. In this section we also discuss the relative contributions of the direct and the various resolved channels. Finally we compare our results with recent preliminary data of the ZEUS collaboration in Sect. 3. A summary and conclusions are given in Sect. 4.

## 2 Comparing Massive and Massless Calculations

In this section we compare the cross sections for  $\gamma + p \rightarrow D^* + X$  in the massless approximation with results from the massive calculation in various kinematical regions which are

relevant for the comparison with recent experimental data. We have chosen to implement the conditions of the ZEUS analysis [2] which are the following: In the HERA ring the energy of the ingoing protons is  $E_p = 920$  GeV and that of the ingoing electrons (positrons)  $E_e = 27.5$  GeV. The total  $\gamma p$  cms-energy  $W$  varies in the range  $130 \text{ GeV} < W < 285$  GeV. We denote the proton four-momentum by  $P$ , the four-momentum of the  $D^*$  by  $p$  and the four-momentum of the virtual photon by  $q$  with  $q^2 = -Q^2$ . The maximal  $Q^2$  in the anti-tagging condition is  $Q^2 < 1 \text{ GeV}^2$ . The transverse momentum distributions are calculated in varying rapidity ( $y$ ) intervals in ten bins of  $p_T$  with the limits as in the ZEUS experiment: 1.9, 2.5, 3.25, 4.0, 5.0, 6.0, 8.0, 10.0, 12.0, 16.0 and 20 GeV. The rapidity intervals are limited by  $-1.6, -0.8, 0.0, 0.8, \text{ and } 1.6$  with the total  $y$  range  $|y| < 1.6$ . In the following, we identify the rapidity  $y$  of the inclusively produced  $c$  quark with the pseudo-rapidity  $\eta$  of the  $D^*$  in the experimental analysis.

Further input for the calculations are the CTEQ6M PDF of the proton [14] and the GRV92 PDF of the photon [15] transformed to the  $\overline{\text{MS}}$  scheme. The fragmentation  $c \rightarrow D^*$  is described by the purely non-perturbative FF [6] (second reference, OPAL set at NLO). The renormalization scale  $\mu_R$  and the factorization scales in the initial and final state,  $\mu_I$  and  $\mu_F$ , are chosen throughout this work as  $2\mu_R = \mu_I = \mu_F = 2\xi m_T = 2\xi \sqrt{p_T^2 + m^2}$  with  $\xi = 1$  except in a study of the scale dependence, where  $\xi$  is varied in the range  $0.5 < \xi < 2$ .  $\alpha_s$  is calculated from the two-loop formula with  $n_f = 4$  and  $\Lambda_{\overline{\text{MS}}}^{(n_f=4)} = 328$  MeV corresponding to  $\alpha_s(m_Z) = 0.118$  and the charm mass is assumed as  $m = 1.5$  GeV. The scale choice for  $\mu_F$  allows us to calculate  $d\sigma/dp_T$  down to small  $p_T$ . For a smaller scale we would come below the starting scale of the FF [6], which is approximately equal to  $2m$ .

We start with a discussion of results for the direct contribution to the cross section for  $\gamma + p \rightarrow D^* + X$  where mass terms proportional to  $m^2/p_T^2$  enter. The mass dependence is located in the cross sections for processes with charm in the final state. These are the parton subprocesses  $\gamma + g \rightarrow c + \bar{c}$  at LO where the gluon originates from the proton; virtual corrections to this process combined with gluon bremsstrahlung  $\gamma + g \rightarrow c + \bar{c} + g$ ; and finally the subprocess  $\gamma + q(\bar{q}) \rightarrow c + \bar{c} + q(\bar{q})$ , where  $q$  denotes a light quark. In addition, the process  $\gamma + c \rightarrow c + g$  including its NLO corrections must be considered. This latter part, however, is calculated with massless charm quarks, as explained above. Explicit expressions for the cross sections and the subtraction terms can be found in our previous work [11].

To study the size of corrections from the mass terms proportional to  $m^2/p_T^2$ , we first look at the direct contribution to  $d\sigma/dp_T$  where we have integrated over the full rapidity range,  $-1.6 \leq y \leq 1.6$ . The result for this differential cross section as a function of  $p_T$  varied between 2.0 and 20 GeV, is shown in Fig. 1a. The curve for  $m \neq 0$  (dashed line) is below the curve for massless  $c$  quarks (full line). On this logarithmic plot, the influence of the non-zero charm mass is visible only for very small  $p_T$ . At  $p_T = 2$  GeV the ratio of the massive to the massless cross section is 0.90 and it approaches 1 very rapidly with increasing  $p_T$ . Actually, the cross section  $d\sigma/dp_T$ , as plotted in Fig. 1a, presents the full

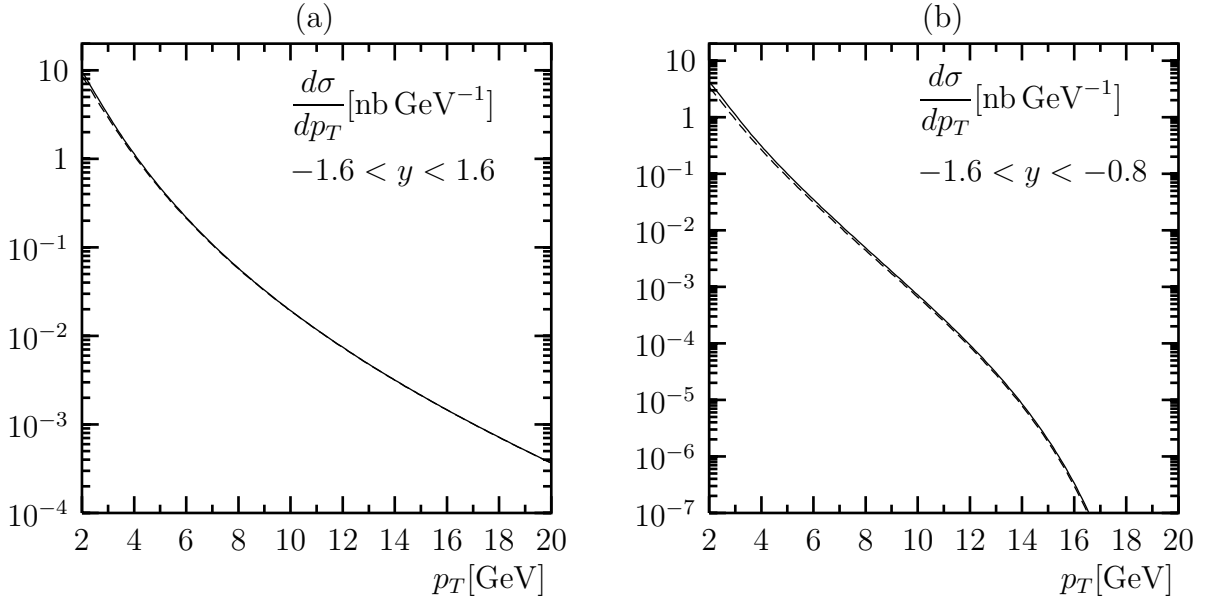


Figure 1: Direct contribution to  $\gamma + p \rightarrow D^* + X$  with massive (dashed lines) and massless charm quarks (full lines) for  $|y| < 1.6$  (a) and  $-1.6 < y < -0.8$  (b).

direct cross section with  $n_f = 4$  flavors, i.e. it contains also the component originating from the  $c$  ( $\bar{c}$ ) in the proton. This component evolves from the factorization of mass singularities at the proton vertex and therefore is evaluated in the massless approximation. However, this contribution is small: at  $p_T = 2$  GeV it amounts to 7.5% in the massless calculation and to 8.4% in the massive case. Without this contribution, the ratio of the massive to the massless cross section would be 0.89. So we conclude that in the direct cross section alone the effect of the charm mass is not negligible at small  $p_T$ . Its effect is strongest for the low- $y$  range. In the four  $y$  regions,  $[-1.6, -0.8]$ ,  $[-0.8, 0.0]$ ,  $[0.0, 0.8]$  and  $[0.8, 1.6]$ , the ratio of the massive to the massless direct cross section at  $p_T = 2$  GeV (full  $n_f = 4$ ) takes the following values: 0.81, 0.86, 0.99, 1.20, as compared to 0.90 over the full  $y$  range. So, depending on the  $y$  range, the non-zero charm mass leads to a change of the direct contribution of approximately 20% at  $p_T = 2$  GeV, in both directions.

The direct cross section  $d\sigma/dp_T$ , integrated over the first  $y$ -interval  $[-1.6, -0.8]$ , is particularly interesting and shown separately in Fig. 1b. As can be seen, the reduction of the massive as compared to the massless cross section is larger than in Fig. 1a. With increasing  $p_T$  the massive cross section does not approach the massless cross section. This is hardly visible in this logarithmic plot, but will be more clearly seen below in a plot for the ratio of the two cross sections. Although interesting from a theoretical point of view, the reduction of the cross section by mass effects at larger  $p_T$  will not become relevant for the comparison with data, since in this region the cross section is too small to be measured: it decreases by 8 orders of magnitude between  $p_T \simeq 2$  GeV and  $p_T \simeq 17$  GeV.

In general, the reduction of the direct cross section due to finite mass effects is significant

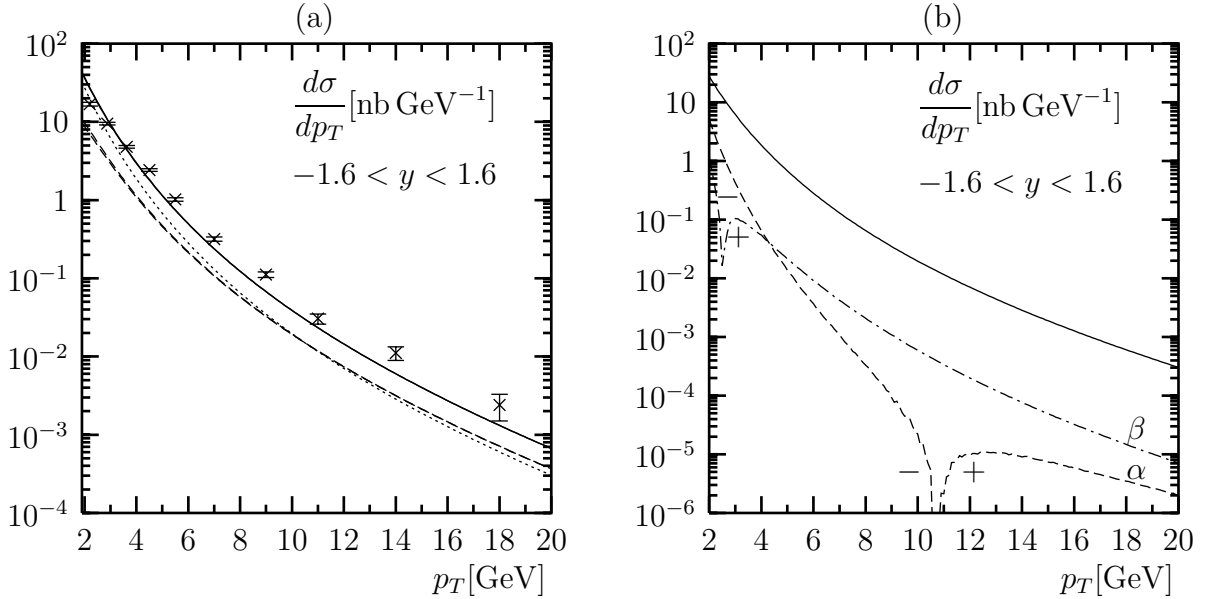


Figure 2:  $p_T$  distribution for  $|y| < 1.6$ . (a) shows the direct (dashed lines) and resolved (dotted line) parts and the sum (full lines) compared with preliminary ZEUS data [2] (only statistical errors are shown). (b) displays separate parts of the resolved contribution (full line):  $\alpha$  is the contribution due to light quarks and gluons in the initial state,  $\beta$  includes in addition charm from the proton.

for  $p_T \lesssim 2$  GeV. It decreases with increasing  $y$ . More details will be shown below when we present the ratios of the massive to the massless cross section as a function of  $p_T$  for the five  $y$  regions. It turns out, however, that in the small  $p_T$  range the resolved contribution is always larger than the direct contribution. This can be seen in Fig. 2a, where we show the direct cross section (dashed lines) for the massless and massive case, the resolved cross section (dotted line), and the sum of both (full line) as a function of  $p_T$ , integrated over the full  $y$  range ( $|y| \leq 1.6$ ). Near  $p_T = 10$  GeV the direct and the resolved contributions cross each other and the direct cross section becomes larger than the resolved one at larger  $p_T$ . One should keep in mind, however, that the direct and resolved parts taken separately are unphysical and scheme dependent; only the sum of both is relevant and can be compared to experimental data. For comparison, the recent preliminary ZEUS data<sup>1</sup> [2] are included in Fig. 2a. As is seen, due to the addition of the resolved contribution, the relative difference between the massless and the massive cross section is very much reduced in the sum, even at small  $p_T$ .

The resolved contributions are due to subprocesses with incoming gluons, light quarks and charm quarks originating from the photon and the proton, including its NLO corrections. Our calculation of the resolved part is based on the work in [16]. The charm quark is treated as a massless particle for these contributions. This is justified since the resolved

<sup>1</sup>Here and below we show only statistical errors. A cross indicates the central value and the statistical error is represented by a vertical line with two horizontal bars.

cross section is dominated by the contribution where the photon resolves into a  $c$  or  $\bar{c}$  and the subprocess cross sections have to be folded with the corresponding charm PDFs. We show the results in detail in Fig. 2b, where different parts of the resolved contribution are plotted separately:  $\alpha$ , the contributions with only light quarks and gluons in the initial state, i.e. processes where  $c$  and  $\bar{c}$  appear in the final state only (dashed line);  $\beta$ , the contribution with charm from the proton added to  $\alpha$  (dashed-dotted line); and the complete resolved cross section with charm from the photon added to  $\beta$  (full line). Here only in the contribution  $\alpha$  the effect of a non-zero charm mass would come into play and  $m^2/p_T^2$  terms are expected to change it for small  $p_T$ . For large  $p_T$  this contribution is extremely small as compared to the complete resolved cross section (more than 2 orders of magnitude smaller for  $p_T > 11$  GeV). For  $p_T \leq 11$  GeV, contribution  $\alpha$  is negative. In absolute value it is below 7% of the sum if  $p_T \geq 3$  GeV and even in the low- $p_T$  range,  $2 < p_T < 3$  GeV, its absolute value amounts to less than 19%. These features are very similar to the results found for the double-resolved cross section for  $\gamma + \gamma \rightarrow D^* + X$  [11]. The dominance of the  $c/\gamma$  contribution in the resolved cross section has been found also in [5] some time ago and is also in accordance with experimental results from ZEUS [17]. There, photoproduction of a  $D^{*\pm}$  in association with one of two energetic jets was measured and clear evidence for the existence of charm coming from the photon was found by measuring the differential cross sections as a function of  $x_\gamma^{obs}$  and as a function of the angle between the charm-jet and the proton beam direction. We remark, that the  $c/p$  contribution (i.e. the difference of parts  $\beta$  and  $\alpha$ ), although small as well, has a stronger fall-off with increasing  $p_T$  than the complete resolved cross section, as to be expected.

To obtain an overview of the non-zero mass effects as a function of  $p_T$  and  $y$ , we present in Fig. 3a-e the ratio of the massive to the massless cross sections integrated over the total  $y$  range,  $|y| < 1.6$ , and for the four separate  $y$  bins,  $y \in [-1.6, -0.8]$ ,  $[-0.8, 0.0]$ ,  $[0.0, 0.8]$ ,  $[0.8, 1.6]$ . First, we show this ratio for the direct contribution originating from light quarks and gluons only (dashed-dotted lines); secondly, we consider the full direct contribution, i.e. with the  $c/p$  part added (dotted lines), which changes this ratio very little; finally, we display the ratio for the complete cross section (full lines), i.e. including the resolved contribution, which, as expected, brings this ratio closer to 1 also for small values of  $p_T$ . For comparison, Fig. 3 shows as well results for the ratio of the LO cross section (sum of direct and resolved parts, dashed lines). These LO results were obtained using the same PDFs, FF and  $\alpha_s$  as in the NLO calculation. Only the NLO corrections in the hard scattering cross sections are left out. Therefore these results are not genuine LO cross sections, where one would use also LO versions of the PDFs, FF and  $\alpha_s$ . In the small  $p_T$  region the ratio for the LO direct part deviates from 1 by less than 10%, whereas the ratio of the full NLO cross sections differs by less than 5% from 1. The fact that at small  $p_T$  this ratio is closer to 1 at NLO than it is at LO, is due to the large NLO corrections in the resolved part. In the last  $y$  bin, it approaches 1 very rapidly with increasing  $p_T$ . For the direct contribution the deviation of the ratio from 1 in the small  $p_T$  region can be compared with the same ratio for the single-resolved contribution for the  $\gamma\gamma$  process [11]. Here the deviation from 1 is somewhat larger. We assume that this

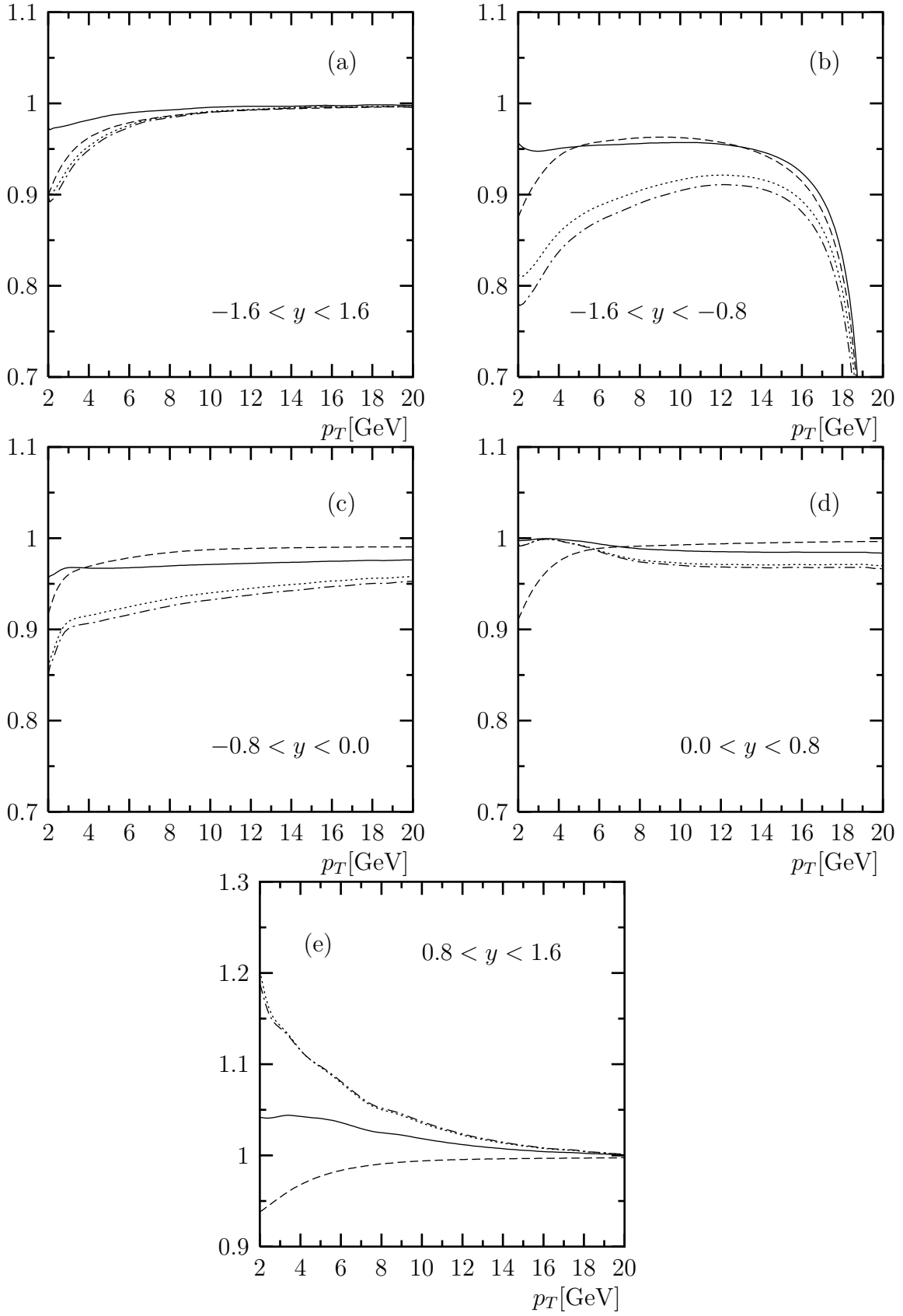


Figure 3: Ratios of massive over massless cross sections  $d\sigma/dp_T$  (see text for details).

is caused by the much harder  $x$  behavior of the gluon PDF of the photon as compared to the very soft small  $x$  behavior of the gluon PDF of the proton.

In the negative  $y$  region the behavior at large  $p_T$  is somewhat different (see Fig. 3b). The strong suppression of the ratio at large  $p_T$  is essentially a phase space effect due to the fact that the lower kinematic limit of  $y$ ,  $y_{\min}$ , increases with increasing  $p_T$ . For fixed  $p_T$  we have

$$y_{\max, \min} = \ln \left( a \pm \sqrt{a^2 - 1} \right) + y_{\text{cms}} \quad (1)$$

with

$$a = \frac{1}{2} \sqrt{\frac{s}{p_T^2 + m^2}}, \quad y_{\text{cms}} = \frac{1}{2} \ln \frac{E_p}{E_e}. \quad (2)$$

This makes  $y_{\min}$  slightly larger for  $m \neq 0$  than for  $m = 0$ . Therefore, the cross section at fixed  $y$ , above but close to  $y_{\min}$ , is smaller for  $m \neq 0$  than for  $m = 0$ . At large  $p_T$ , only part of the small- $y$  bin is kinematically allowed. For example, at  $p_T = 19$  GeV,  $y_{\min} \simeq -1.06$ . As a consequence, the ratio of massive over massless cross sections decreases at large  $p_T > 10$  GeV (see Fig. 3b). We repeat that this peculiar mass effect will not be relevant for the comparison with experimental data, since the cross section in this  $y$  bin is very small at large  $p_T$ . However, even for  $p_T < 10$  GeV the ratio stays constant with a value  $\simeq 0.95$  so that phase space limitation effects reduce the resulting cross section in the massive theory for all  $p_T$  and for  $-1.6 < y < -0.8$  by at least 5%.

A trace of this effect is visible even for the  $y$  bin  $[-0.8, 0.0]$  shown in Fig. 3c. Here the ratio stays below 1 over the whole  $p_T$  range. It deviates from 1 still at the largest  $p_T$  by  $\simeq 3\%$ . The behavior of the ratio in the  $y$  bin  $[0.0, 0.8]$  is similar (see Fig. 3d).

It is well-known that for photoproduction processes it is very important to perform the calculations at least up to NLO. NLO contributions reduce the overall scale dependence, but also have a strong influence on the absolute normalization of the cross sections. The effect of NLO corrections on the hard scattering cross sections is different for the direct and the resolved components and depends on the kinematic variables like  $y$  and  $p_T$ . To study this dependence we have calculated the ratio  $K = d\sigma/dp_T(\text{NLO})/d\sigma/dp_T(\text{LO})$ , where the LO cross section is defined in the same way as described above. The  $K$  factors for the five  $y$ -bins and in the full region  $|y| < 1.6$  are exhibited in Fig. 4a-e. The  $K$  factors are smaller for the direct than for the resolved parts. For the complete cross section,  $K$  is in general below 2. In the first  $y$  bin ( $y \in [-1.6, -0.8]$ ), however,  $K$  increases strongly with increasing  $p_T$  for  $p_T > 10$  GeV. Here the NLO corrections are so large that one may have doubts concerning the perturbative stability. Again, this is mainly a kinematic effect, since in the first  $y$ -bin  $y_{\min}$  increases with  $p_T$  and cuts out most of the  $y$  region in this bin.

To obtain an estimate of the theoretical error we varied the common value of the renormalization scale and the factorization scales for initial and final state singularities. We have chosen to vary  $\xi$  as defined above between 0.5 and 2. The result for  $d\sigma/dp_T$  integrated over the full  $y$  range,  $|y| < 1.6$ , is plotted in Fig. 5.  $\xi = 0.5$  (2) is for the upper (lower) and  $\xi = 1$  for the middle curves. The scale variation of the direct contribution

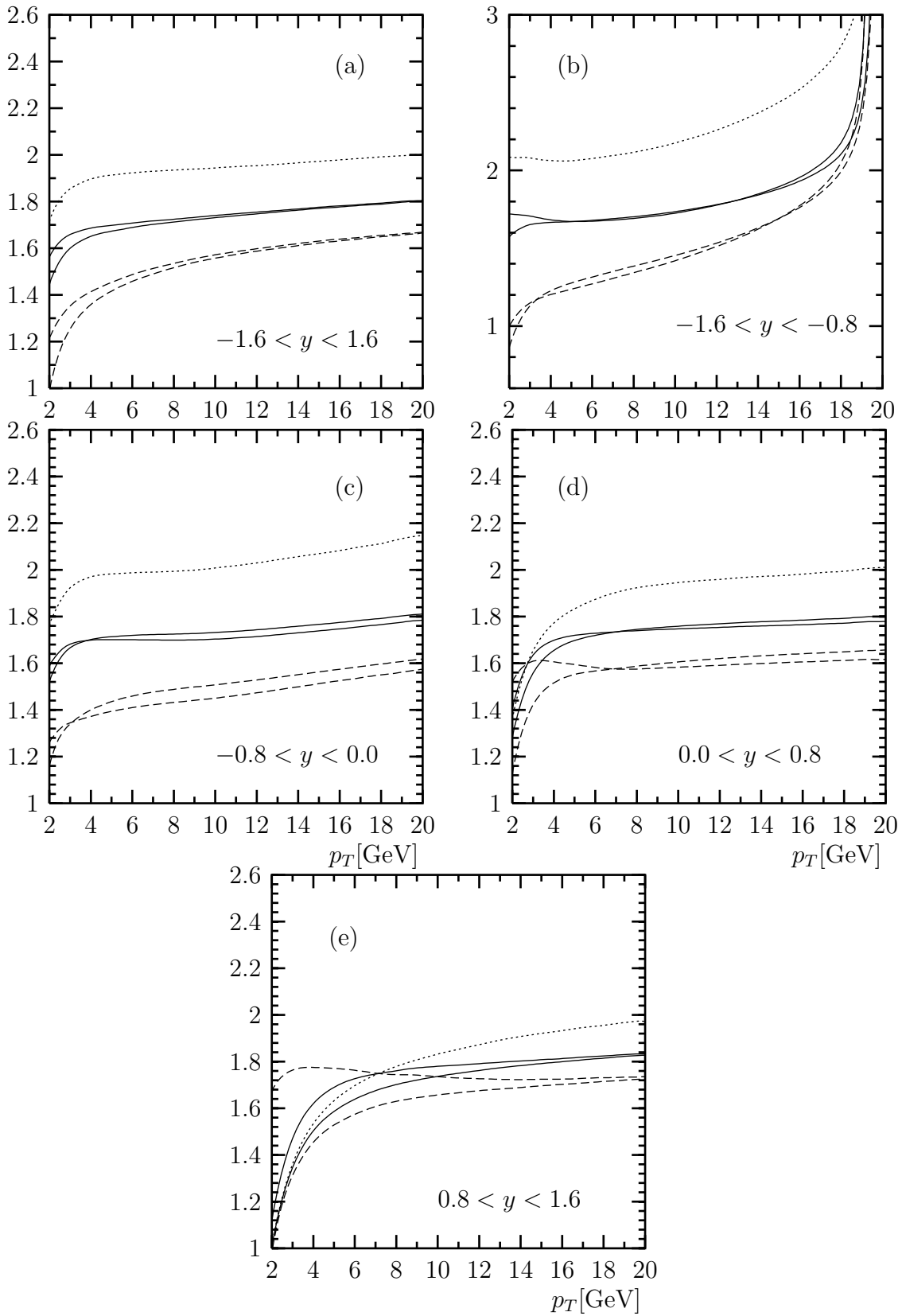


Figure 4:  $K$  factors for the cross sections  $d\sigma/dp_T$ . Dashed lines are obtained from the direct massless (lower curves at low  $p_T$ ) and direct massive calculations (upper curves at low  $p_T$ ). Dotted lines are for the resolved contribution and full lines correspond to the full cross section (again the massless and massive approaches corresponding to lower and upper curves at low  $p_T$ ).

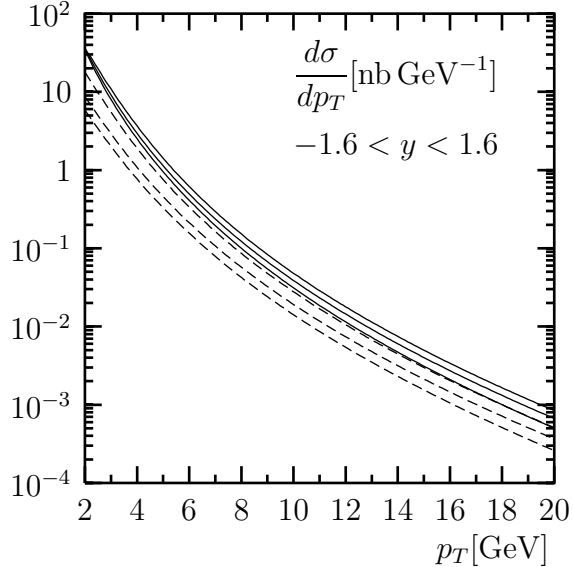


Figure 5: The complete cross section (full lines) and the direct contribution (dashed lines) with varied factorization and renormalization scales  $2\mu_R = \mu_I = \mu_F = 2\xi\sqrt{p_T^2 + m^2}$ ,  $\xi = 0.5$  (upper), 1.0 (middle) and 2.0 (lower curves).

in the massive version is shown separately (dashed lines). By adding the resolved cross section the scale variation is reduced, in particular for small  $p_T$ . This results mainly from a compensation between the scale dependence of the photon PDF entering the resolved LO contribution and the scale dependence of NLO corrections to the direct cross section<sup>2</sup>.

### 3 Comparison with Preliminary ZEUS Data

In this section we compare our results with preliminary experimental data from the ZEUS collaboration at HERA [2]. There exist similar data from the H1 collaboration [3] with somewhat different kinematical constraints which we have not used in this work.

When comparing predictions for the  $p_T$ -distributions with the experimental results, we show both the differential cross section  $d\sigma/dp_T$  as a function of  $p_T$ , as well as the values averaged over the  $p_T$ -bins as used by ZEUS. The comparison for the  $p_T$ -distributions in the five  $y$  bins,  $y \in [-1.6, 1.6]$ ,  $[-1.6, -0.8]$ ,  $[-0.8, 0.0]$ ,  $[0.0, 0.8]$ ,  $[0.8, 1.6]$  is shown in Fig. 6a-e. In all five figures, the three continuous curves are for the massive direct (dashed lines), the resolved (dotted lines) and the complete (full lines) cross sections. The agreement

<sup>2</sup>This estimate differs from the one in [2] where scale variations were chosen independently for  $\mu_R$ ,  $\mu_I$  and  $\mu_F$  over the range  $0.5 < \xi < 2$  and the maximal positive/negative changes for all possible combinations of scales was used to estimate a theoretical error. Consequently, the error turned out to be largest at small  $p_T$ . We note that at very small  $p_T$  the scale with  $\xi = 0.5$  is below the starting scale of the  $D^*$  FF so that the FF does not vary anymore with the scale.

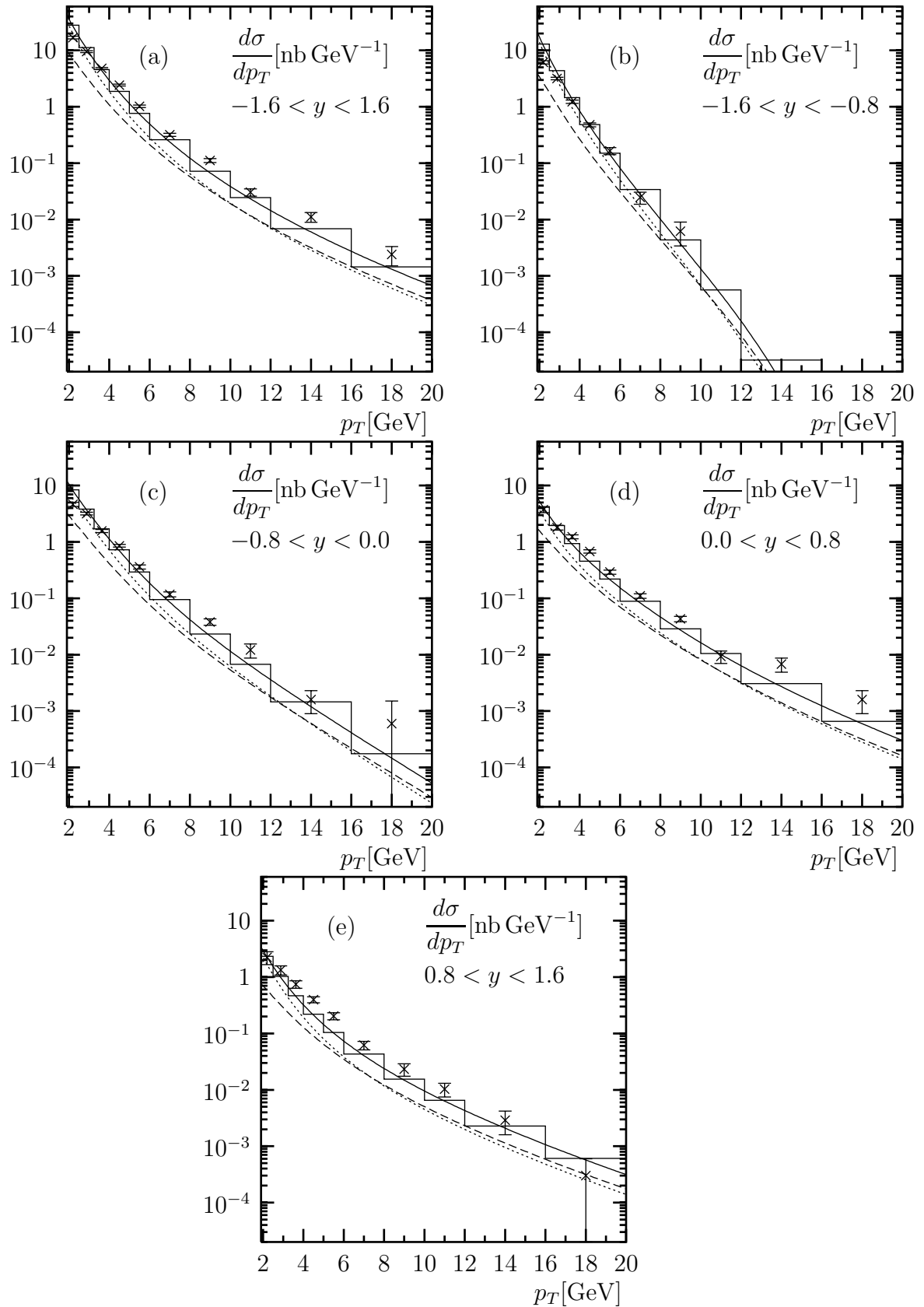


Figure 6:  $p_T$  distributions in various  $y$ -bins compared with preliminary ZEUS data [2] (only statistical errors shown), see text for further details.

between data and theory is quite good if one takes into account the theoretical error due to the scale variation shown above in Fig. 5. Only in the first  $p_T$  bin and for negative  $y$ , the data points are lower than the predictions (Fig. 6b, c). Also for the full  $y$  range,  $|y| < 1.6$ , the prediction at the smallest  $p_T$  is too high (Fig. 6a). It is conceivable that in this low- $p_T$ -region the massive theory with  $n_f = 4$  loses its validity and one must switch to the FFN theory with  $n_f = 3$ . In the two bins with positive  $y$ , where the cross section is smaller, we find good agreement also for low  $p_T$ .

Comparing Figs. 3b, c with Figs. 6b, c, it is clear that mass effects can not be made responsible for the differences between data and theoretical predictions. In the two bins with negative  $y$  the massive theory resulted in cross sections smaller than the massless theory by 5%. But this is not sufficient to bring the prediction into agreement with the data. At intermediate values of  $p_T$ , the data tend to be above the calculation. These deviations are more important at large  $y$  and do not appear as prominent after averaging over the full  $y$ -range.

Non-zero charm mass corrections are expected to be relevant only for small  $p_T$  values. Corresponding differences may become visible only in the lowest  $p_T$ -bin. On the other hand, the total cross section, as well as distributions with respect to other kinematic variables, are dominated by low  $p_T$ . Therefore we consider in the following the differential cross sections  $d\sigma/dy$ ,  $d\sigma/dW$  and  $d\sigma/dz$ , where  $z$  is the inelasticity  $z = Pp/Pq$ , only for the case with  $p_T$  integrated over the full range  $1.9 < p_T < 20$  GeV. Equivalent results with different  $p_T$  ranges (like  $3.25 - 5.0$ ,  $5.0 - 8.0$  or  $8.0 - 20$  GeV as measured in [2]) are expected to show good agreement with predictions of the massless theory. Corresponding

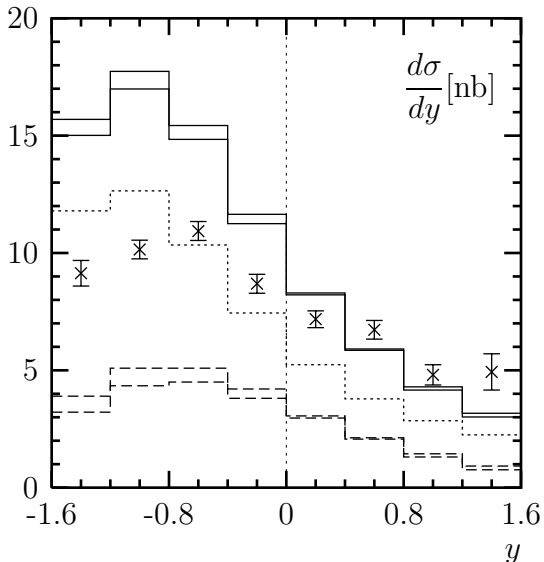


Figure 7: Rapidity distribution compared with preliminary ZEUS data for  $1.9 \text{ GeV} < p_T < 20 \text{ GeV}$  (only statistical errors shown), see text for further details.

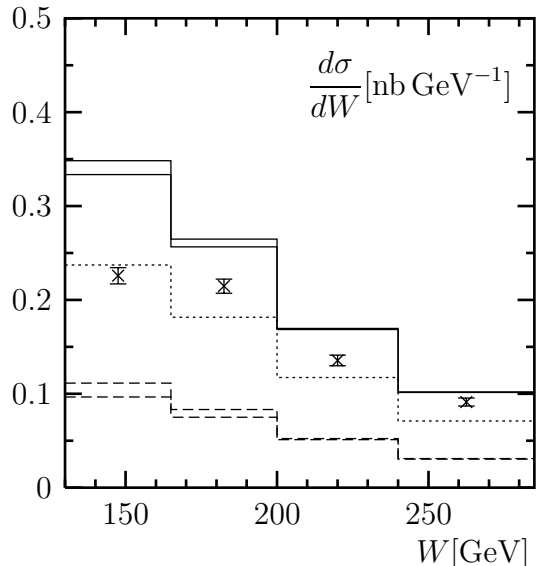


Figure 8:  $W$  distribution compared with preliminary ZEUS data for  $1.9 \text{ GeV} < p_T < 20 \text{ GeV}$  and  $|y| < 1.6$  (only statistical errors shown), see text for further details.

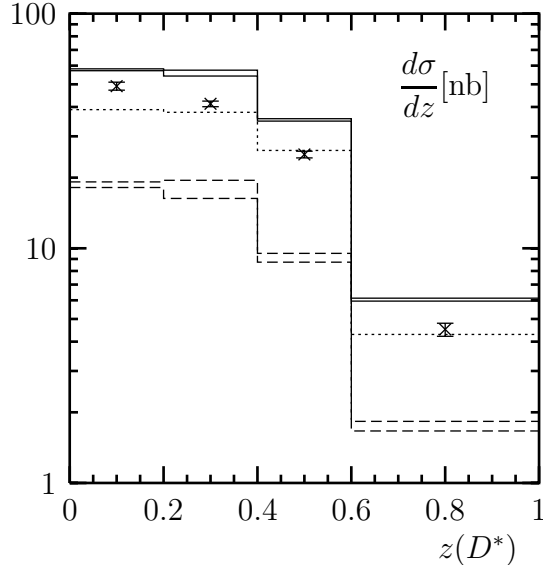


Figure 9:  $z(D^*)$  distribution compared with preliminary ZEUS data for  $1.9 \text{ GeV} < p_T < 20 \text{ GeV}$  and  $|y| < 1.6$  (only statistical errors are shown), see text for further details.

comparisons are shown in [2]. Our results for the massive and the purely massless theory are presented in Figs. 7, 8 and 9 together with the preliminary data points from ZEUS [2]. In all figures, full lines are used to display to the sum of the direct (dashed lines) and resolved (dotted lines) parts; upper and lower lines correspond to the massless and massive calculations. We have chosen bins in  $y$ ,  $W$  and  $z$  in the same way as in the experimental analysis.  $d\sigma/dy$  agrees approximately with the data for  $y > 0$ , but not for  $y < 0$ . Therefore, the latter region is responsible for the disagreement with the data in the first  $p_T$  bin in Figs. 6b and c and also in Fig. 6a. In the region  $y > 0$ , the corrections due to the non-zero charm mass are negligibly small. For  $y < 0$  these corrections are larger, but not large enough to account for the difference with the data. In the plot for  $d\sigma/dW$  the corrections compared to the massless version are below 5% in all  $W$  bins. The agreement with the data is better for larger  $W$ . For  $d\sigma/dz$  (Fig. 9), the mass corrections are very small, since the resolved part is equally dominating in all  $z$ -bins.

## 4 Summary and Conclusions

In this paper we have compared two approaches for the calculation of inclusive  $D^*$  photoproduction. One approach uses massless charm quarks and the usual  $\overline{\text{MS}}$  factorization, the second is based on a calculation with massive charm quarks and subsequent absorption of the logarithmic mass dependence into the charm parton distribution and fragmentation functions.

In the direct part of the cross section the non-zero mass corrections were fully taken into

account. For this purpose subtraction terms, established already previously in connection with a study of  $\gamma\gamma \rightarrow D^*X$ , have been applied. They allowed us to combine the massive calculation in a consistent way with the parton distributions of the photon and the proton and with fragmentation functions of the  $c$  quark into  $D^*$  defined in the  $\overline{\text{MS}}$  factorization scheme. In this modified massive theory the cross sections converge in general rapidly to their massless limits with increasing  $p_T$ . Only at rather small  $p_T$ , terms proportional to  $m^2/p_T^2$  are important and produce deviations from the massless theory of up to 20% at the smallest  $p_T$  considered. In the negative rapidity region the convergence of the massive to the massless theory is disturbed at large  $p_T$  by finite charm mass corrections in the value of the kinematic boundary for the rapidity. This has the effect that over the full range of  $p_T$  the non-zero mass corrections are larger than 10%. The contribution with the charm quark coming from the proton is very small.

The resolved contribution has two parts. One originates from light quarks and gluons in the initial state, the other comes from an initial charm quark in the photon and/or the proton. The contribution with charm coming from the photon overwhelms the resolved cross section by far and for consistency is calculated with massless quarks. Since the part with charm quarks only in the final state is negligible, except possibly for very small  $p_T$ , the total resolved cross section is also evaluated with massless charm quarks. Consequently, finite charm mass effects are found in the direct part only. The studies with zero and non-zero charm mass have been done for kinematic ranges as in a recent ZEUS analysis of  $D^*$  photoproduction measurements.

For the comparison with these recent ZEUS data we added the direct and resolved cross sections. The agreement of our predictions with the data is quite good, in particular for the  $p_T$  distributions down to  $p_T \simeq 3$  GeV. Non-zero charm mass effects are not essential even at small  $p_T$ , since in this region the cross section is dominated by the resolved cross section. To improve the theory at very small  $p_T$  it seems necessary to switch from the four-flavor to the three-flavor theory. The agreement with the experimental distributions with respect to the rapidity,  $W$ , and  $z$ , is not so good. Here the theoretical predictions might improve by trying other PDFs of the photon, in particular for the charm part, which dominates the cross section in the low- $p_T$  range.

## Acknowledgement

We thank B. A. Kniehl and M. Spira for providing us with programs for the calculation of the resolved contributions. We also thank L. Gladilin for helpful discussions about the preliminary data of the ZEUS collaboration.

## References

- [1] S. Frixione, M. Mangano, P. Nason and G. Ridolfi, Phys. Lett. B348, 633 (1995); S. Frixione, P. Nason and G. Ridolfi, Nucl. Phys. B545, 3 (1995) and earlier references given there
- [2] ZEUS Collaboration, S. Chekanov et al., 31st International Conference on High Energy Physics, ICHEP02, July 24-31 2002, Amsterdam, Abstract 786; see also: ZEUS Collaboration, [http://www-zeus.desy.de/public\\_plots](http://www-zeus.desy.de/public_plots), "Measurement of D\* photoproduction at HERA", 2003
- [3] H1 Collaboration, International Europhysics Conference on High Energy Physics, EPS03, July 17-23 2003, Aachen, Abstract 097, DESY-H1prelim-03-071 and earlier H1 papers given in this reference
- [4] M. Cacciari and M. Greco, Z. Phys. C69, 459 (1996); Phys. Rev. D55, 7134 (1997)
- [5] B. A. Kniehl, G. Kramer and M. Spira, Z. Phys. C76, 689 (1997)
- [6] J. Binnewies, B.A. Kniehl and G. Kramer, Z. Phys. C76, 677 (1997); Phys. Rev. D58, 014014 (1998)
- [7] W. K. Tung, S. Kretzer and C. Schmidt, J. Phys. G28, 983 (2002) and earlier papers given there
- [8] J. Collins, Phys. Rev. D58, 094002 (1998)
- [9] H. L. Lai et al., Eur. Phys. J. C12, 375 (2000)
- [10] S. Kretzer, H. L. Lai, F. I. Olness and W. K. Tung, MSU-HEP-030101, BNL-NT-03/2, RBRC-325, hep-ph/0307022
- [11] G. Kramer and H. Spiesberger, Eur. Phys. J. C22, 289 (2001); Eur. Phys. J. C28, 495 (2003)
- [12] M. Krämer, F. I. Olness and D. E. Soper, Phys. Rev. D62, 096007 (2000)
- [13] M. Cacciari, S. Frixione and P. Nason, JHEP 0103, 006 (2001); S. Frixione and P. Nason, JHEP 0203, 053 (2002)
- [14] J. Pumplin et al., JHEP 0207, 012 (2002)
- [15] M. Glück, E. Reya and A. Vogt, Phys. Rev. D46, 1973 (1992)
- [16] F. Aversa, P. Chiappetta, M. Greco, J. P. Guillet, Nucl. Phys. B327, 105 (1989); B. A. Kniehl, G. Kramer, M. Spira, Z. Phys. C76, 689 (1997); J. Binnewies, B. A. Kniehl, G. Kramer, Z. Phys. C76, 677 (1997)

- [17] ZEUS Collaboration, J. Breitweg et al., *Eur. Phys. J C*6, 67 (1999); ZEUS Collaboration, S. Chekanov et al., *Phys. Lett. B*565, 87 (2003)